2013

Modelling and Configuration Control of Wing-Shaped Bi-Stable Piezoelectric Composites Under Aerodynamic Loads

Andres F. Arrieta

Onur Bilgen
Old Dominion University

Michael I. Friswell

Paolo Ermanni

Original Publication Citation

Arrieta, A. F., Bilgen, O., Friswell, M. I., & Ermanni, P. (2013). Modelling and configuration control of wing-shaped bi-stable piezoelectric composites under aerodynamic loads. *Aerospace Science and Technology, 29*(1), 453-461. doi:10.1016/j.ast.2013.05.004

Aerospace Science and Technology 29 (2013) 453–461

Contents lists available at SciVerse ScienceDirect

Aerospace Science and Technology

www.elsevier.com/locate/aescte

Modelling and configuration control of wing-shaped bi-stable piezoelectric composites under aerodynamic loads

Andres F. Arrieta [a,*], Onur Bilgen [b], Michael I. Friswell [c], Paolo Ermanni [a]

[a] Centre of Structure Technologies, ETH Zurich, Leonhardstrasse 27, Zurich, CH-8092, Switzerland
[b] Old Dominion University, Department of Mechanical and Aerospace Engineering, Norfolk, VA 23529, USA
[c] College of Engineering, Swansea University, Singleton Park, Swansea, SA2 8PP, UK

ARTICLE INFO

Article history:
Received 11 December 2012
Received in revised form 23 April 2013
Accepted 9 May 2013
Available online 20 May 2013

Keywords:
Bi-stable wing
Unsymmetric composite
Morphing
Snap-through

ABSTRACT

Bi-stable composites have been considered for morphing applications thanks to their ability to hold two statically stable shapes with no energy consumption. In this paper, the modelling of the dynamic response of cantilevered wing-shaped bi-stable composites is presented. To this end, an analytical model approximating the dynamic response about each statically stable shape of wing-shaped bi-stable composites is derived. Theoretical modal properties are obtained to attain or stabilise a desired configuration following a previously introduced resonant control strategy. The resonant control technique is evaluated for a wing-shaped bi-stable composite subject to aerodynamic loads. Wind tunnel experiments are conducted on a wing-shaped specimen showing the ability of the control strategy to stabilise or attain a desired stable shape under aerodynamic loads.

1. Introduction

Bi-stable composites are structures capable of adopting two statically stable configurations [11]. The bi-stability property has drawn considerable attention from the adaptive structure community for its potential applications in morphing structures, as no energy is required to hold each of the stable configurations [10]. Multi-stability arises due to an induced stress field in the composite laminates that can result from several mechanisms, including unsymmetrical lamination [12], tailored lay-up [17], pre-stressed cylinders [13], fibre pre-stressing [8] and thickness variation [9]. The change between stable states is physically realised as a jump phenomenon known as snap-through, which is strongly nonlinear in nature [2]. Different actuator systems and techniques have been previously used to trigger snap-through. Shape memory wires successfully achieved reversible changes between the stable states of bi-stable composites, however suffered of integration problems and reduced control bandwidth [7]. Quasi-static actuation employing piezoelectric elements led to achieving snap-through only in one direction, nevertheless reversing the configuration to the original state was not possible due to insufficient actuation authority [19,16]. The recently introduced idea of exploiting the rich dynamics of bi-stable composites to enhance the actuation authority showed encouraging results [3,20]. In this context, Arrieta et al. [1] presented the implementation and demonstration of purely piezoelectric material dynamically induced forward and reverse snap-through of a bi-stable unsymmetric composite plate with a clamped edge. This resonant actuation strategy provided for the first time full configuration control of $[0_n/90_n]$ cantilevered bi-stable composites under the sole action of piezoelectric actuators.

The implementation of multi-stable components in adaptable aerodynamic structures has the potential to reduce actuation requirements as energy is not required to hold a largely deformed shape. Hence, significant deflections can be achieved spending energy only to trigger a snap-through from the original stable state to another. As with any active or semi-active compliant aerodynamic surface, a bi-stable piezoelectric composite wing is practical if sufficient aerodynamic load carrying capability in each state and bi-directional snap-through using relatively low excitation voltages are achieved. Such structures can be realised by careful selection of actuator placement, boundary conditions and laminate lay-up, coupled with the developed resonant control morphing strategy.

An analytical model to obtain the modal frequencies for wing-shaped bi-stable composites is presented in this paper. The accurate prediction of the modal properties of such structures allows the application of the previously introduced resonant control technique which has been shown to enable full configuration control on bi-stable composites. A wing-shaped bi-stable composite specimen actuated with Macro-Fiber Composite (MFC) actuators is used to demonstrate this concept under the presence of aerodynamic loads. The use of MFC actuators allows the exploitation of the higher actuation authority obtained from the d_{33} coupling coefficient, by using interdigitated electrodes which guide the electrical field along the longitudinal direction of the fibres [27]. The d_{33}

* Corresponding author.
E-mail address: andresar@ethz.ch (A.F. Arrieta).

1270-9638
http://dx.doi.org/10.1016/j.ast.2013.05.004

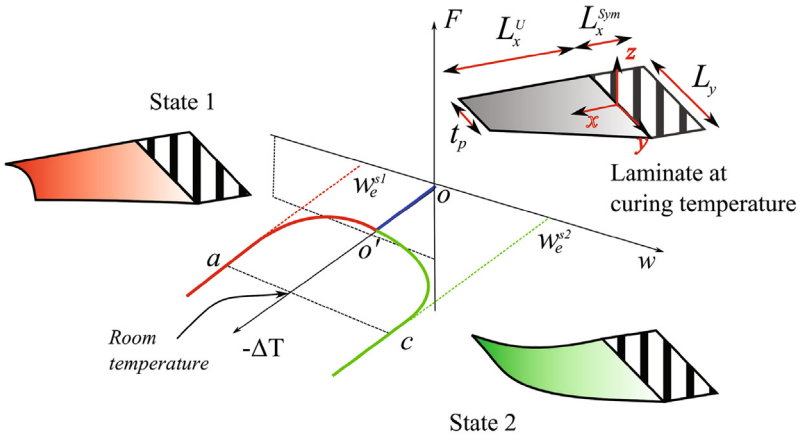

Fig. 1. Bifurcation diagram showing the statically stable configurations of a bi-stable composite. Equilibrium points a and c lying on the red and green branches correspond to the resulting shapes of State 1 and 2, respectively. (For interpretation of the references to colour in this figure legend, the reader is referred to the web version of this paper.)

coefficient is larger than the conventionally used d_{31} coupling coefficient. To achieve morphing control between the stable shapes, a model for the dynamics of the wing-shaped bi-stable composites about the statically stable shapes is developed. To this end, an analytical model approximating the linear dynamics for wing-shaped bi-stable composites about the predicted stable configuration is derived. This model allows to calculate the modal characteristics of wing-shaped bi-stable composites, which are crucial for the correct application of the resonant control technique. Furthermore, the analytical model allows the selection of the position piezoelectric actuators for maximum control authority in the required modes. The parametric nature of the presented model allows for efficient sensitivity analyses and initial rapid optimisation to be carried out, while nonlinear finite element methods [23,24] can be used for final refinements at a later design stage. An experimental characterisation is conducted using frequency response functions (FRF) validating the results obtained with the derived model. The aerodynamic response of a tapered bi-stable wing-shaped specimen is tested, showing the capabilities of the resonant actuation strategy to control the configuration even against a certain level of adverse pressure gradient. This characteristic allows for using such bi-stable structures in morphing winglets applications. The paper concludes with a brief summary of the presented results and discussion of possible applications.

2. Modelling of bi-stable composites

In this study, laminates with a tapered planform arranged in a cantilever configuration are studied. To achieve this, a tailored lay-up with symmetrical and unsymmetrical stacking sequences is used [14]. Bi-stability arises due to the unsymmetrically laminated part, as thermal stresses resulting from a mismatch between the thermal expansion coefficients of the fibres and the epoxy matrix are induced during cool down after curing. This process is schematically shown in Fig. 1, where w is the out-of-plane displacement, ΔT is the difference between the curing and the actual temperatures, and F is the external load. Initially at the curing temperature, the flat laminate configuration starts from point C_o^o from which it cools down reaching the bifurcation point $C_o^{o'}$, i.e. following path $C_o^o\vec{C}_o^{o'}$. At the bifurcation point, the cool down process can continue in either of the two stable branches until it reaches an equilibrium at room temperature, this is through path $C_o^{o'}\vec{C}_a^o$ to equilibrium point C_a^o, or through path $C_o^{o'}\vec{C}_c^o$ to equilibrium point C_c^o. At room temperature, changes between the stable states are caused by forcing a large deflection on the laminate triggering a snap-through [2]. The modelling of the shapes resulting from the bifurcation process and the dynamics around these stable configurations are presented in the following.

2.1. Variational formulation

A variational formulation is followed for the calculation of the final equilibrium shapes and the associated dynamic response of the studied wing-shaped bi-stable composites is presented. The Lagrangian, $\mathcal{L}$, for a bi-stable composite is equivalent to that of a cross-ply unsymmetrically laminated plate given by:

$$\mathcal{L} = T - U + \mathcal{W}_{ext}, \tag{1}$$

where T, U are the kinetic and potential energies, and $\mathcal{W}_{ext}$ is the work done by external energy, respectively.

The kinetic energy of the system is the sum of the kinetic energy of the composite and the piezoelectric elements, given by:

$$T_s = \frac{1}{2}\int_{V_s} \rho \dot{\mathbf{u}}'\dot{\mathbf{u}}\, dV_s, \tag{2}$$

and

$$T_{pzt} = \frac{1}{2}\sum_{k=1}^{Npzt}\int_{V_p^{(k)}} \rho_{pzt}\dot{\mathbf{u}}'\dot{\mathbf{u}}\, dV_p^{(k)}, \tag{3}$$

where the displacement field vector is defined as $\mathbf{u} = [u(x, y, t), v(x, y, t), w(x, y, t)]'$, ρ and ρ_{pzt} are the density of the composite and the piezoelectric elements, respectively, V_s and $V_p^{(k)}$ are the volume of the composite and the kth piezoelectric element, respectively, N_{pzt} is the total number of piezoelectric elements bonded to the bi-stable composite, the overdot $(\dot{})$ symbol implies differentiation with respect to time, and the superscript $(')$ indicates the transpose operation.

The total kinetic energy is thus written as:

$$T = T_s + T_{pzt}. \tag{4}$$

The strain energy of the bi-stable plate is obtained by summing the contributions of the symmetrical and unsymmetrical parts of the lay-up, yielding:

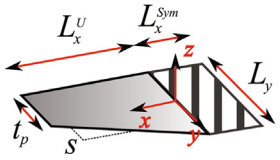

Fig. 2. Planform defining the domain of integration for the bi-stable wing.

$$U_s = \int_{-L_x^{Sym}}^{0} \int_{\frac{-L_y}{2}}^{\frac{L_y}{2}} \frac{1}{2} \left(\begin{bmatrix} \boldsymbol{\epsilon^o} \\ \boldsymbol{\kappa} \end{bmatrix}'_{Sym} \begin{pmatrix} \mathbf{A} & \mathbf{B} \\ \mathbf{B} & \mathbf{D} \end{pmatrix}_{Sym} \right) \begin{bmatrix} \boldsymbol{\epsilon^o} \\ \boldsymbol{\kappa} \end{bmatrix}_{Sym} dy\,dx + \int_{0}^{L_x^U} \int_{\frac{-L_y}{2}}^{sx+\frac{L_y}{2}} \frac{1}{2} \left(\begin{bmatrix} \boldsymbol{\epsilon^o} \\ \boldsymbol{\kappa} \end{bmatrix}'_{U} \begin{pmatrix} \mathbf{A} & \mathbf{B} \\ \mathbf{B} & \mathbf{D} \end{pmatrix}_{U} - \begin{bmatrix} \mathbf{N_T} \\ \mathbf{M_T} \end{bmatrix}' \right) \begin{bmatrix} \boldsymbol{\epsilon^o} \\ \boldsymbol{\kappa} \end{bmatrix}_{U} dy\,dx, \tag{5}$$

where $\boldsymbol{\epsilon^o} = [\epsilon^o_{xx}\ \epsilon^o_{yy}\ \epsilon^o_{xy}]'$ is the vector of in-plane strains, $\boldsymbol{\kappa} = [\kappa_{xx}\ \kappa_{yy}\ \kappa_{xy}]'$ is the vector of bending strains, and **A**, **B**, **D** represent the well known extensional, bending–extension coupling, and bending stiffness matrices, respectively, and $\mathbf{N_T}$ and $\mathbf{M_T}$ are the thermal expansion force and moment vectors, respectively [22]. The subscripts $_{Sym}$ and $_U$ indicate symmetric and unsymmetric lamination, respectively. The planform dimensions defining the integration domain are given by the span of the unsymmetric region, L_x^u, the length of the symmetric region, L_x^{Sym}, the chord length at the clamped edge, L_y, and the chord length of the tip, t_p. The leading-edge slope defining the wing-shaped (tapered) form is given by $s = \frac{t_p - L_y}{L_x^U}$. A detailed geometrical description of the planform is presented in Fig. 2. The total strain is given by $\epsilon_{ij} = \epsilon^o_{ij} + z\kappa_{ij}$. Note that the symmetrical part does not exhibit resulting thermal stresses. The nonlinear extensional strain and bending curvatures, ϵ^o_{ij} and κ_{ij}, respectively, are given by:

$$\epsilon^o_{xx} = \frac{\partial u}{\partial x} + \frac{1}{2}\left(\frac{\partial w}{\partial x}\right)^2, \tag{6}$$

$$\epsilon^o_{yy} = \frac{\partial v}{\partial y} + \frac{1}{2}\left(\frac{\partial w}{\partial y}\right)^2, \tag{7}$$

$$\epsilon^o_{xy} = \frac{\partial u}{\partial y} + \frac{\partial v}{\partial x} + \frac{\partial w}{\partial x}\frac{\partial w}{\partial y}, \tag{8}$$

and,

$$\kappa_{xx} = -\frac{\partial^2 w}{\partial x^2}, \tag{9}$$

$$\kappa_{yy} = -\frac{\partial^2 w}{\partial y^2}, \tag{10}$$

$$\kappa_{xy} = -2\frac{\partial^2 w}{\partial x \partial y}. \tag{11}$$

The piezoelectric strain energy and the internal electrical work are given by:

$$U_{pzt} = \frac{1}{2}\sum_{k=1}^{Npzt} \int_{V_p^{(k)}} \mathbf{S}'_p \mathcal{T}\, dV_p^{(k)} + \frac{1}{2}\sum_{k=1}^{Npzt} \int_{V_p^{(k)}} \boldsymbol{E}_3 \mathcal{D}_3\, dV_p^{(k)}, \tag{12}$$

where $\mathbf{S}_p$ is the vector of strains, $\mathcal{T}$ is the vector of material stress. The poling and extension directions of the piezoelectric elements, 3, coincides with the in-plane x-direction, consistent with the MFC actuators that are employed. A state of plane stress is assumed for the considered structures, thus the components of the stress and strain vector for piezoelectric materials are related by the constitutive relations:

$$\begin{bmatrix} \sigma_{11} \\ \sigma_{22} \\ \sigma_{12} \\ \mathcal{D}_3 \end{bmatrix} = \begin{pmatrix} c^E_{11} & c^E_{12} & 0 & -e_{33} \\ c^E_{12} & c^E_{22} & 0 & -e_{31} \\ 0 & 0 & g^E_{12} & 0 \\ e_{33} & e_{31} & 0 & \varepsilon^S_{33} \end{pmatrix} \begin{bmatrix} \epsilon_{11} \\ \epsilon_{22} \\ \epsilon_{12} \\ E_3 \end{bmatrix}, \tag{13}$$

where σ_{ij} is total stress due to a strain in the i-direction acting on the j-direction, ϵ_{ij} is mechanical strain due to a deflection in the i-direction acting on the j-direction, $\mathcal{D}_3$ is electrical displacement in the 3-direction, E_3 is the electric field in the 3-direction, c^E_{ij} is the elastic modulus due to a strain in the i-direction acting on the j-direction, g^E_{ij} is the shear modulus due to a strain in the i-direction acting on the j-direction, e_{ij} is the piezoelectric constant relating the poling direction i with the strain in the j-direction, and ε^S_{33} is the permittivity coefficient relating the electrical displacement in the 3-direction with the poling direction of the piezoelectric material, respectively. The superscripts E and S denote that the relevant parameters are measured at constant electric field and constant strain, respectively. The total strain energy for the system is thus written as:

$$U = U_s + U_{pzt}. \tag{14}$$

2.2. Equilibrium configurations

The room temperature shapes of the static equilibrium points are obtained by minimising the potential energy of the laminate U_s. To approximate the large transverse static deflections due to the cooling process the following polynomial shape functions are used:

$$u^o(x,y) = \sum_{i=1}^{N}\sum_{j=1}^{N} a_{ij} x^i y^{j-1}, \tag{15}$$

$$v^o(x,y) = \sum_{i=1}^{N}\sum_{j=1}^{N} b_{ij} x^i y^{j-1}, \tag{16}$$

$$w^o(x,y) = \sum_{i=1}^{N}\sum_{j=1}^{N} c_{ij} x^{i+1} y^{j-1}, \tag{17}$$

where $u^o(x,y)$, $y^o(x,y)$ and $w^o(x,y)$ are the mid-plane displacements defining the static equilibrium shapes, $a_{ij}x^i y^j$, $b_{ij}x^i y^j$, and $c_{ij}x^i y^j$ are the shape functions on each coordinate direction, and, $N \times N$ gives the total number of shape functions used on each expansion. It is necessary to impose continuity of the displacement to account for the interaction of the symmetric and unsymmetric parts of the laminate. This is achieved by satisfying the following conditions on the displacements:

$$u^o_{Sym}(0,y) = u^o_U(0,y), \tag{18}$$

$$v^o_{Sym}(0,y) = v^o_U(0,y), \tag{19}$$

$$w^o_{Sym}(0,y) = w^o_U(0,y), \tag{20}$$

$$\frac{\partial w^o_{Sym}(0,y)}{\partial y} = \frac{\partial w^o_U(0,y)}{\partial y}. \tag{21}$$

Substituting Eqs. (6)–(11) and Eqs. (15)–(17) into Eq. (5) the equilibrium shapes are found from:

$$\frac{\partial U}{\partial \alpha_i} = 0, \tag{22}$$

where $\alpha = [a_{ij}, b_{ij}, c_{ij}]$ is the vector of generalised static displacements. The stability of the equilibrium points, C^o_k, is obtained by

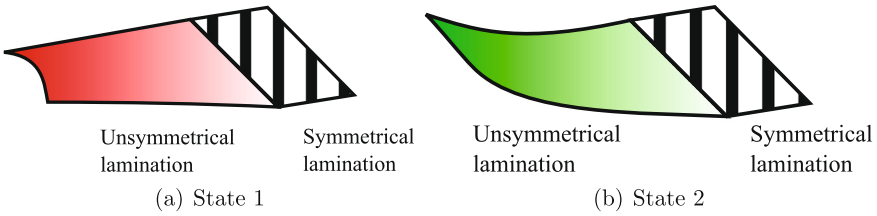

Fig. 3. Statically stable configurations of a tapered bi-stable composite wing.

evaluating the definiteness of the associated Hessian matrix, which is:

$$\frac{\partial^2 U_s}{\partial \alpha_i \alpha_j} = H_k|_{C_k^o}. \tag{23}$$

Minima of the potential energy indicate statically stable shapes, which are given by equilibrium points with positive definite Hessian matrix. Maxima and saddle equilibria are indicated by the Hessian matrix evaluated at the respective equilibrium points being negative definite and indefinite, respectively. The resulting geometry for the statically stable equilibrium configurations are given by the mid-plane displacements $u_o(x, y, t)$, $y_o(x, y, t)$ and $w_o(x, y, t)$ of the equilibrium points having a positive definite Hessian matrix, which are schematically shown for points a and c in Figs. 3(a) and 3(b), respectively. Hereafter, all calculations shown in this study occur about the stable equilibria reached at room temperature. It is worth mentioning that the final equilibrium shapes are a function of the composite material properties, lamination sequence, curing cycle, and the dimensions of the initially flat laminate. Hence, these quantities may be optimised to achieve tailored dynamic and aerodynamic characteristics for a particular application.

2.3. Linear dynamic response modelling

The study of the dynamic behaviour of the wing-shaped piezoelectric bi-stable composites is focused on the low amplitude response around the stable equilibrium configurations. This assumes a linear approximation of the behaviour using the equilibrium points found in Section 2.2. Hence, the linear dynamics are obtained as perturbations about the static displacements of the stable shapes given by $u_o(x, y, t)$, $y_o(x, y, t)$ and $w_o(x, y, t)$ [26]. As a result, the linear approximation of the vibration problem reduces to that of a tapered unsymmetrically laminated shell solved for each stable equilibrium point. In the following derivation, first the associated low amplitude linear vibration problem about a single stable state is solved using the Ritz method. This allows us to obtain natural frequencies and mode shapes for comparison with experimentally measured quantities and for the optimal positioning of actuators. For the dynamic morphing strategy for bi-stable composite structures used in this study, as shown in Ref. [1], knowledge of linear modal properties is sufficient to utilise the resonant actuation strategy and achieving full configuration control. The equilibrium shapes of bi-stable composites resembles that of thin-walled shells having a small transverse displacement to span ratio, thus the principal curvatures are small. Practically, this implies that Cartesian coordinates x and y may be selected as the curvilinear coordinates for the middle surface from where the displacements for bi-stable composites are defined. Hence, shallow shell theory is adopted [25].

For the linear approximation problem following the above described perturbation approach, the membrane strains are recast as:

$$\epsilon_{xx}^o = \frac{\partial u}{\partial x} + \frac{w_o}{R_x(x, y)}, \tag{24}$$

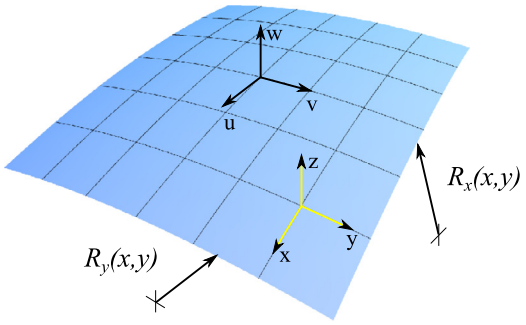

Fig. 4. Shell element showing curvilinear coordinates (x, y), radii of curvature and displacements $u(x, y, t)$, $y(x, y, t)$ and $w(x, y, t)$. The radii of curvature are orientated in the principal x-, y-directions; however their magnitudes at each point (defining the mid-surface) are a function of the coordinates.

$$\epsilon_{yy}^o = \frac{\partial v}{\partial y} + \frac{w_o}{R_y(x, y)}, \tag{25}$$

$$\epsilon_{xy}^o = \frac{\partial u}{\partial y} + \frac{\partial v}{\partial x}, \tag{26}$$

where the radii of curvature in the x- and y-directions are $R_x(x, y)$ and $R_y(x, y)$, respectively as shown in Fig. 4. In the case at hand, the radii of curvature R_x and R_y are defined by the large amplitude static displacements of the each equilibrium shapes given by Eq. (22). The bending curvatures remain unchanged as defined in Eqs. (9)–(11).

The types of shells studied in this investigation are cantilever tapered bi-stable composites, i.e. one edge clamped and the remaining three being free. In this case, the clamping device imposes a prescribed curvature at the root of the wing-shaped composite. The employed tailored lay-up exhibiting symmetrical and unsymmetrical regions makes possible such clamped configuration. There exists no known closed-form solutions for this type of linear shell vibration problem [18]. An approximate solution is hence obtained following the Ritz method, for which admissible functions satisfying the geometric boundary conditions for the displacements are chosen. A set of basis functions offering a good compromise between accuracy and relatively fast converge whilst satisfying the above stated boundary conditions are:

$$u(x, y, t) = \sum_{i=1}^{M}\sum_{j=1}^{M} a_{ij} x^i y^{j-1} u_{i,j}(t), \tag{27}$$

$$v(x, y, t) = \sum_{i=1}^{M}\sum_{j=1}^{M} b_{ij} x^i y^{j-1} v_{i,j}(t), \tag{28}$$

$$w(x, y, t) = \sum_{i=1}^{M}\sum_{j=1}^{M} c_{ij} x^{i+1} y^{j-1} w_{i,j}(t), \tag{29}$$

where $u_{ij}(t)$, $v_{ij}(t)$ and $w_{ij}(t)$ are time response coefficients to be determined, $a_{ij}x^i y^j$, $b_{ij}x^i y^j$, and $c_{ij}x^i y^j$ are the shape functions on each coordinate direction, and, $3 \times M \times M$ gives the total number of degrees of freedom in the dynamic analysis.

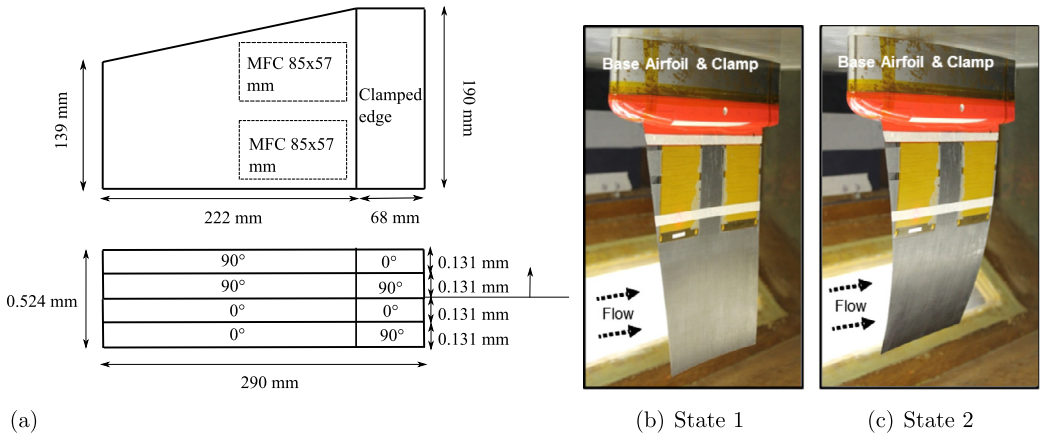

Fig. 5. (a) Planform illustration of the bi-stable wing. (b, c) Bi-stable wing clamped on the base airfoil and mounted in the test section. Two MFC M-8557-P1 type actuators are bonded to the lower surface of the bi-stable wing.

In the current formulation, the piezoelectric elements are assumed to be perfectly bonded to the surface of the bi-stable composite and the electric field is taken as the independent variable in the electrical domain. Based on the assumption that the d_{33} electromechanical coupling coefficient of the MFC P1 type actuator can be represented by an effective d_{31} electromechanical coupling coefficient, one electrical degree of freedom per element is sufficient for modelling the electrical response [5]. The effective electric field of the kth piezoelectric element is thus written as:

$$E_{3k}(x, y, t) = \frac{1}{\Delta_{el}} \mathrm{v}_k(t), \tag{30}$$

where $\mathrm{v}_k(t)$ is the generalised voltage time coordinate of the kth piezoelectric element, and Δ_{el} is the spacing between electrodes [6].

The linear equations of motion for the tapered piezoelectric bi-stable composites are obtained using Lagrange's equations for the mechanical and electrical displacements, yielding:

$$\frac{d}{dt}\left(\frac{\partial \mathcal{L}}{\partial \dot{q}_a}\right) - \frac{\partial \mathcal{L}}{q_a} = F_{aext}, \tag{31}$$

$$\frac{d}{dt}\left(\frac{\partial \mathcal{L}}{\partial \dot{\mathrm{v}}_b}\right) - \frac{\partial \mathcal{L}}{\mathrm{v}_b} = Q_{bext}, \tag{32}$$

where the generalised coordinates q_a and v_b are the time response coefficients for the mechanical and the electrical displacements. Back substituting Eqs. (27)–(30) until Eq. (1) is reached into Eqs. (31) and (32), yields the electromechanical equations of motion for piezoelectric bi-stable composite wings as:

$$\mathbf{M}\ddot{\mathbf{q}} + \mathbf{K}\mathbf{q} - \boldsymbol{\Theta}\mathbf{v} = \mathbf{f}_{ext}, \tag{33}$$

$$\boldsymbol{\Theta}'\mathbf{q} + \mathbf{C_p}\mathbf{v} = \boldsymbol{\varphi}_{ext}, \tag{34}$$

where $\mathbf{q}$ is the mechanical displacement vector given by $\mathbf{q} = [u_{ij}(t), v_{ij}(t), w_{ij}(t)]'$, $\mathbf{v}$ is the electrical displacement vector given by $\mathbf{v} = [\mathrm{v}_k(t)]'$, $\mathbf{f}_{ext}$ is the mechanical external forcing vector, and $\boldsymbol{\varphi}_{ext}$ is the external electrical forcing vector. $\mathbf{M}$, $\mathbf{K}$, $\boldsymbol{\Theta}$ and $\mathbf{C_p}$, are the mass, stiffness, electromechanical coupling and capacitive matrices of the piezoelectric bi-stable composite, respectively.

In this study, the piezoelectric elements are used as actuators driven by a voltage source independent of the dynamics of the system, whereas the external mechanical forcing is given by the aerodynamic pressure on the wing-like bi-stable composite. Hence, the electrical equation given by Eq. (34) can be dropped and the voltage term in Eq. (33) becomes the control input to the system. The modal characteristics are obtained from studying the homogeneous vibration problem, i.e. assuming zero voltage in the electrodes of the piezoelectric elements, no aerodynamic force and a harmonic response $\mathbf{q} = \boldsymbol{\nu} e^{\mathrm{i}\omega t}$, given by:

$$\left(\mathbf{K} - \omega^2 \mathbf{M}\right)\boldsymbol{\nu} = 0, \tag{35}$$

where $\boldsymbol{\nu}$ is the vector of amplitudes, ω are the eigenvalues of the problem, and i is the imaginary number. Eq. (35) is solved to obtain eigenvalues, which are equivalent to modal frequencies for the problem at hand. The eigenvalues obtained with Eq. (35) are compared to experimentally measured modal frequencies. Furthermore, eigenvalues serve as upper bounds for the modal frequencies in the design of wing-shaped bi-stable composites. The electromechanical equations of motion for the linear problem given in Eq. (33) can be manipulated to obtain low amplitude frequency response functions (FRF) by applying the Fourier transform of the mechanical displacement and electrical vectors, $\mathcal{F}[\mathbf{q}] = \mathrm{A}(\mathrm{i}\varpi)$ and $\mathcal{F}[\mathbf{v}] = \mathrm{V}(\mathrm{i}\varpi)$, respectively. The piezoelectric forcing to displacement FRF, $\mathrm{H}(\mathrm{i}\varpi)$, for no external input $F_{ext} = 0$ (latex syntax) is obtained as:

$$\frac{\mathrm{A}(\mathrm{i}\varpi)}{\mathrm{V}(\mathrm{i}\varpi)} = \mathrm{H}(\mathrm{i}\varpi) = \left(\mathbf{K} - \omega^2 \mathbf{M}\right)^{-1} \boldsymbol{\Theta}. \tag{36}$$

The obtained linear electromechanical equations of motion are useful in two important aspects. First, given the geometry of the bi-stable composite structure the modal properties, namely natural frequencies and mode shapes, for the electromechanical system can be obtained with Eqs. (33) and (34). Second, the electromechanical coupling matrix can be studied as a function of the position of the piezoelectric elements allowing for maximisation of the actuation authority for specific modes. This is however beyond the scope of the current work.

3. Structural dynamic response

In this section the structural dynamic response of a bi-stable wing-like composite is conducted, i.e. under no aerodynamic influence, $f_{ext} = 0$. The obtained results are used to validate the presented theoretical model.

3.1. Experimental set-up

The test specimen for the structural and aerodynamic investigations is a bi-stable composite with a tapered wing planform laid-up having two distinct stacking sequences, as shown in detail in Fig. 5(a). The symmetrically laminated smaller portion is designed to allow the composite to be clamped. A carbon fibre-epoxy prepreg, type E022-T700 manufactured by SGL [21], is used for

Table 1
Geometric properties of the wetted area of the bi-stable piezocomposite wing in two different stable equilibria.

State	Designation	Span location [mm]	Chord [mm]	Camber [%c]
1	Root	68	190	1.8
	Laser-line	143	171	2.1
	Mid-span	175	163	2.2
	Tip	290	139	2.9
2	Root	68	190	1.6
	Laser-line	143	171	0.3
	Mid-span	175	163	0.0
	Tip	290	139	0.7

each layer. The Macro-Fiber Composite (MFC) actuators are used to excite the bi-stable plate. Two MFC M8557-P1 type actuators are bonded near the base of the bi-stable plate on the lower "pressure" surface of the wing. As shown in Fig. 5, the fibres on the lower surfaces are oriented at 0° which corresponds to the span axis. In order to maximise the out-of-plane bending induced by the MFC actuator, the piezoceramic fibres of the MFC must be close to the effective neutral plane of the unsymmetric cross-ply laminate and the plate must be compliant in bending and stiff in in-plane extension. The analysis of thin MFC actuated structures is presented in [5] and the results from that analysis is used to aid the design in the current research. In the case studied here, the out-of-plane deflection induced on the bi-stable plate by the unidirectional in-plane actuation of the MFC actuator is maximised by bonding the MFC actuator directly on the lower layer with zero degree (spanwise) fibre orientation.

The geometric features of the wetted bi-stable wing are presented in Table 1.

3.2. Frequency response and modal properties

Dynamic tests to evaluate the modal response of the studied bi-stable wing were conducted and compared to analytical results. An LTC-300-200-SA laser displacement sensor and a Siglab 20-22 frequency analyser was used to measure the single-point displacement of the complete wing structure mounted in the wind tunnel. A chirp signal was used to obtain FRF measurements, where the excitation was a sine tone with continuously varying frequency in a selected range. The control signal to the MFC actuators was amplified using a TREK 2220 high voltage amplifier. The experiments were conducted at a single excitation voltage level of 200 Vac which is assumed to be in the linear actuation regime. Particular attention is placed in the range where the first bending modes of each stable configuration are located. In this paper, State 1 is defined as the stiff state and it has a major curvature mainly along the chord axis. The effect of curvature in State 1 is analogous to the effect of camber. State 2 is defined as the compliant state and it has a major curvature mainly along the span axis. The effect of curvature in State 2 is analogous to the effect of dihedral. Experimental and simulated FRFs for stable State 1 are compared showing good agreement in Fig. 6(a). Only the viscous damping coefficient is tuned using the experimentally measured value. The resonance frequency of the first bending mode in State 1, w_1^{s1}, is experimentally observed at 30.1 Hz closely matched by the theoretical result of 31.0 Hz. Similar results for State 2 can be seen in Fig. 6(b), showing good agreement between the experimental first bending mode of State 2, w_1^{s2}, found at 13.1 Hz compared to the theoretical result of 14.1 Hz. For both State 1 and State 2, the stiffer approximation of the analytical method is observed and expected.

The resonant strategy is tested without the presence of aerodynamic loads, showing the ability of the chosen actuators to dynamically trigger snap-through from either stable state. Multi-event snap-through in bi-stable composites is previously been reported and modelled in literature for slowly applied loads [15]. In the context of configuration control under aerodynamic loads multi-event snap-through is not observed. These results are omitted for brevity; the interested reader is referred to Ref. [1] for details.

4. Aerodynamic response

The passive aerodynamic characteristics of the test specimen are evaluated first. A detailed study of the aerodynamic response of the tested bi-stable wing-shaped composites is presented in [4]. To this end, the bi-stable wing is attached to the balance system in the wind tunnel through an airfoil base, as shown in Fig. 5. This has a NACA 0012 profile and transfers the aerodynamic loads to the moment arm of the wind tunnel load balance system. This consists of two sections. The upper section, adjacent to the root of the complete wing, is a solid steel NACA 0012 airfoil with 254 mm chord. The lower section, adjacent to the root of the bi-stable plate, is a multi-part clamping mechanism also having a NACA 0012 profile in two planes.

Fig. 5 shows the bi-stable piezoelectric composite wing clamped to the base airfoil. The aerodynamic response is studied by varying the free-stream velocity and the angle of attack (AOA) to simulate the working environment for such a structure. More precisely, the pressure distribution is mainly varied via the AOA and the net pressure acting on the wing is mainly varied by the free-stream velocity. The first goal is to demonstrate the fact that the structure can sustain a certain level of adverse pressure gradient without snapping to another state. This property shows the passive load carrying capability of the bi-stable wing. The critical values of

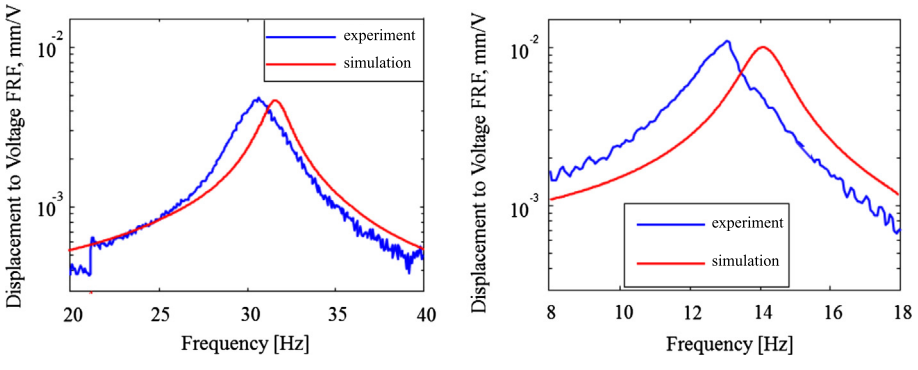

Fig. 6. Comparison between experimental and simulated single-point out-of-plane displacement to harmonic voltage excitation FRF, $H(i\varpi)$, of the bi-stable piezocomposite wing clamped to the base airfoil and mounted on the wind tunnel load balance. Vpeak = 200 Vac. (a) State 1, (b) State 2.

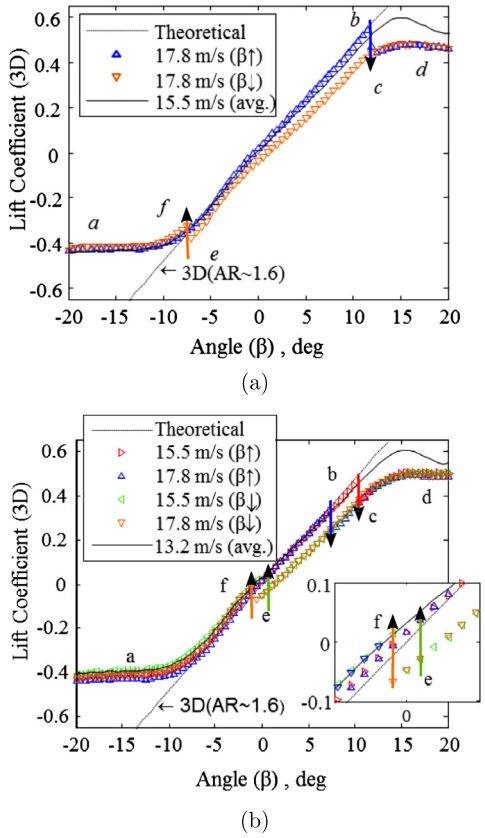

Fig. 7. Experimental (3D) aerodynamic response for active bi-stable wing to rotation angle, β, and free-stream velocity. Coloured arrows indicate the direction of snap-through for each AOA sweep. (a) Passive, (b) active with excitation at 13.0 Hz, 800 Vac. (Colour online.)

snap-inducing velocity and AOA are key values in determining the passive load carrying capability. It should be noted that the pitch angle, β, determined by the rotary table in the set-up, is selected as the independent variable since the calculation of the geometric AOA of the 3D structure in the wind tunnel is impractical with the available sensors. First, the critical free-stream velocity and angle of attack that induce snap-through from State 1 to State 2 are examined. These values are obtained through a set of AOA sweeps conducted in the range of 10 to 20 m/s nominal velocity values, where the velocity range is swept in 2.5 m/s steps. The AOA sweep is conducted, in both directions, in the range of $-20°$ to $+20°$ varying the AOA in 0.5° steps. Snap-through may occur if the net pressure, primarily controlled by the free-stream velocity, is high enough in the AOA range that is examined; therefore a critical free-stream velocity also exists for a preselected range of AOA. Below the critical free-stream velocity, a state can be passively held for the entire AOA range that is of interest. Snap-through is induced by the dynamic pressure if the critical velocity is exceeded. Fig. 7(a) presents the aerodynamic response of the bi-stable plate at two different free-stream velocities where the AOA is first swept up from $-20°$ to $+20°$ and swept back down to $-20°$. The wing is set at State 1 which is the favourable state at $-20°$ AOA. As noted above, five velocity values are examined; however only two important velocity values are presented. Fig. 7(a) also presents the theoretical finite-wing lift curve for reference. A snap-through is not observed for the complete AOA range, in both directions, at 15.5 m/s and all other velocities below this critical value. Due to the lack of aerodynamic hysteresis, the AOA up and down sweeps are averaged and presented as a single curve for the 15.5 m/s velocity test. In contrast, at 17.8 m/s, snap-through is observed in both direction as expected – indicating that the critical velocity value is in the range of 15.5 to 17.8 m/s. The path *abcdefa* is indicated in the figures to aid the discussion. An adverse pressure gradient sustained by the specimen develops from the angle at which the lift coefficient changes sign until the load carrying capability of the specimen is lost when a snap-through is triggered. This can be observed by following the AOA sweeps in Fig. 7(a).

The second type of aerodynamic measurements on the bi-stable wing, following a similar experimental procedure as described above, is conducted to understand the actively induced snap-through that is caused by the MFC actuators. The goal here is to demonstrate that the structure can be made, effectively, monostable against a certain level of adverse pressure gradient. This property shows the controllability of a desired state achieved with the embedded MFC actuators under the presence of aerodynamic forces. The critical values of voltage excitation amplitude and frequency are key in determining the controllability property. First, a sinusoidal excitation with 800 Vac amplitude at 13.0 Hz is applied which corresponds to the resonance frequency of State 2 following the used resonant control strategy. This excitation causes the wing to be effectively monostable for State 1. Fig. 7(b) presents the aerodynamic response of the bi-stable plate at three different free-stream velocities where the AOA is first swept up from $-20°$ to $+20°$ and swept back down to $-20°$ for the active case. The path *abcdefa* is indicated in the figures to aid the discussion. As in Fig. 7(a), the wing is set at State 1 which is the favourable state at $-20°$ AOA. A snap-through is not observed for the complete AOA range, in both directions, at 13.2 m/s and all other velocities below this critical velocity value. Due to the lack of aerodynamic hysteresis, the AOA up and down sweeps are averaged and presented as a single curve for the 13.2 m/s velocity test. In contrast, at 15.5 and 17.8 m/s, snap-through is observed in both directions as expected indicating that the critical velocity value is in the range of 13.2 to 15.5 m/s. (Note: If a gust causes the wing to go from State 1 to State 2, snap-through from State 2 to State 1 is always guaranteed for velocities below the critical velocity independent of the AOA.) In contrast to the passive structure, a dynamically induced snap-through from State 2 to State1 is observed near zero degree of the mount angle where the pressure gradient is near neutral for the lower 15.5 m/s velocity (see the path *ef* in Fig. 7(b)). The snap-through occurs at $-0.5°$ and 0.0° for the velocities of 17.8 and 15.5 m/s respectively indicating that the dynamic excitation can achieve snap-through from State 2 to State 1 by tailoring the composite and optimising the distribution of actuation even against a certain level of adverse gradient.

Similar results are obtained for the aerodynamic characteristics and morphing control under the presence of flow induced pressure for State 2. Fig. 8(a) presents the aerodynamic response of the passive structure for free-stream and AOA sweeps first starting down from $+20°$ to $-20°$ and swept back up to $+20°$. The wing is set at State 2 which is the favourable state at $+20°$ AOA due to pressure gradient. The response for the AOA high–low–high sweep is very similar to the previously presented AOA low–high–low sweep. A snap-through is not observed for the complete AOA range, in both directions, at 15.5 m/s and all other velocities below this critical value. Due to the lack of aerodynamic hysteresis, the AOA up and down sweeps are averaged and presented as a single curve for the 15.5 m/s velocity test. In contrast, at 17.8 m/s, snap-through is observed in both direction as expected, indicating that the critical velocity value is in the range of 15.5 to 17.8 m/s. For this case, the range of AOA for which an adverse pressure gradient develops is found as explained above. Fig. 8(b) presents the free-stream and AOA sweeps of the dynamically excited bi-stable plate at three different free-stream velocities where the AOA is first swept down from $+20°$ to $-20°$ and swept back up to $+20°$. A sinusoidal excitation with 1000 Vac amplitude at 30.0 Hz and 300 Vdc offset is applied – the excitation frequency is near the

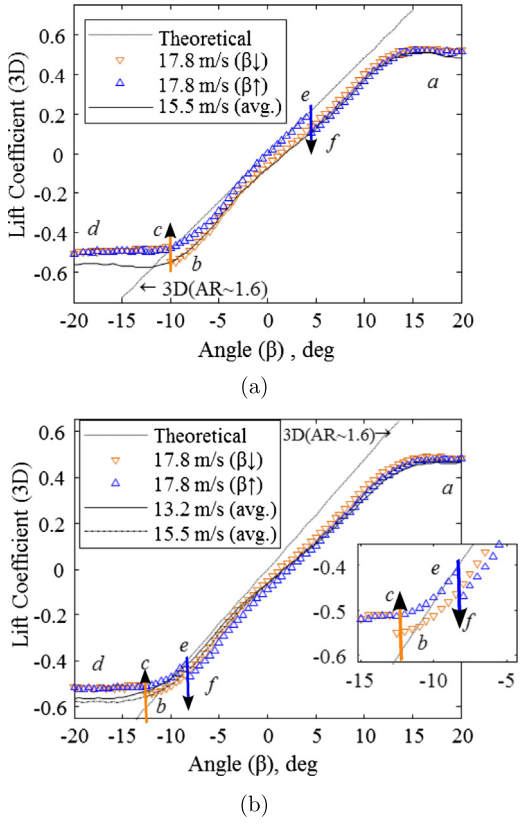

Fig. 8. Experimental (3D) aerodynamic response for active bi-stable wing to rotation angle, β, and free-stream velocity. Coloured arrows indicate the direction of snap-through for each AOA sweep. (a) Passive, (b) active with excitation at 30.0 Hz, 1000 Vac. (Colour online.)

resonance frequency of State 1. The response for the AOA high–low–high sweep is different than the previously presented AOA low–high–low sweep. A snap-through is not observed for the complete AOA range, in both directions, at 13.2 and 15.5 m/s and all other velocities below the value of 13.2 m/s. Due to the lack of aerodynamic hysteresis, the AOA up and down sweeps are averaged for the 13.2 and 15.5 m/s velocity tests. In contrast, at 17.8 m/s, snap-through is observed in both directions indicating that the critical velocity value is in the range of 15.5 to 17.8 m/s. In the case where State 2 is the desired state, the dynamic excitation is clearly capable of achieving State 2 in the presence of adverse pressure gradient (see the path *ef* in Fig. 8(b)) before it is triggered aerodynamically (see path *ef* in Fig. 8(a)).

5. Conclusions

The modelling for the dynamics and the aerodynamic response of a wing-like bi-stable composite laminate are presented. An analytical model using the Ritz method is developed yielding important modal properties for bi-stable wing-shaped composites. This analytical model allows the design of geometrical features in order to obtain desired modal characteristics for each stable state. These are crucial to conduct a resonant actuation strategy allowing to control the configuration of the bi-stable wing. Furthermore, the theoretical modal frequencies provided by the model can be used to optimise the positioning of the MFC actuators to achieve improved actuation authority by maximising the generalised electromechanical coupling coefficients for the modes to be controlled. This is the subject of future work. The aerodynamic characteristics of a wing specimen are studied in order to test the resonant actuation strategy against a dynamic pressure. It is demonstrated that full configuration control using only MFC actuators is achieved, even against an adverse dynamic pressure. The shown passive load carrying capabilities and the presented control strategy to stabilise each state of the wing-shaped bi-stable specimen allows for the possible application of such structures as morphing winglets. The load carrying capability of the presented wing-shaped bi-stable composite concept can be substantially increased by using thicker laminates. Moreover, the control strategy exploiting the inertial advantage from resonance allows for limiting the increase in actuation requirements. Further gains in performance can be achieved by designing the positioning of the MFC actuators taking into account the passive aerodynamic behaviour of the bi-stable wing structure. The presented results show the possibility to implement wing-shaped bi-stable composite in shape adaptable aerodynamic structures, such as winglets.

Acknowledgements

The authors would like to thank the support of the ETH Research Commission and the Marie Curie Actions Cofund Program; Dr. A.F. Arrieta is funded through an ETH Postdoctoral Fellowship. The authors also acknowledge the support received from the European Research Council (ERC). The research leading to these results has received funding from the ERC under the European Union's Seventh Framework Programme (FP/2007–2013)/ERC Grant Agreement No. [247045].

References

[1] A.F. Arrieta, O. Bilgen, M.I. Friswell, P. Hagedorn, Dynamic control for morphing of bi-stable composites, Journal of Intelligent Material Systems and Structures 24 (3) (2012) 266–273.
[2] A.F. Arrieta, S.A. Neild, D.J. Wagg, On the cross-well dynamics of a bi-stable composite plate, Journal of Sound and Vibration 330 (14) (2011) 3424–3441.
[3] A.F. Arrieta, D.J. Wagg, S.A. Neild, Dynamic snap-through for morphing of bi-stable composite plates, Journal of Intelligent Material Systems and Structures 22 (2) (2011) 103–112.
[4] O. Bilgen, A.F. Arrieta, M.I. Friswell, P. Hagedorn, Dynamic control of a bistable wing under aerodynamic loading, Smart Material and Structures 22 (2) (2013) 025020.
[5] O. Bilgen, A. Erturk, D.J. Inman, Analytical and experimental characterization of macro-fiber composite actuated thin clamped-free unimorph benders, Journal of Vibration and Acoustics 132 (5) (2010) 051005.
[6] O. Bilgen, Y. Wang, D.J. Inman, Electromechanical comparison of cantilevered beams with multifunctional piezoceramic devices, Mechanical Systems and Signal Processing 27 (3) (2012) 763–777.
[7] M.L. Dano, M.W. Hyer, SMA-induced snap-through of unsymmetric fiber-reinforced composite laminates, International Journal of Solids and Structures 40 (22) (2003) 5949–5972.
[8] S. Daynes, K.D. Potter, P.M. Weaver, Bistable prestressed buckled laminates, Composites Science and Technology 68 (9) (2008) 3431–3437.
[9] S. Daynes, P.M. Weaver, J.A. Trevarthen, A morphing composite air inlet with multiple stable shapes, Journal of Intelligent Material Systems and Structures 22 (9) (2011) 961–973.
[10] C.G. Diaconu, P.M. Weaver, F. Mattioni, Concepts for morphing airfoil sections using bi-stable laminated composite structures, Thin-Walled Structures 46 (6) (2008) 689–701.
[11] M.W. Hyer, Some observations on the cured shapes of thin unsymmetric laminates, Journal of Composite Materials 15 (15) (1981) 175–194.
[12] M.W. Hyer, Calculations of the room-temperature shapes of unsymmetric laminates, Journal of Composite Materials 15 (1981) 296–310.
[13] E. Kebadze, S.D. Guest, S. Pellegrino, Bistable prestressed shell structures, International Journal of Solids and Structures 41 (11–12) (2004) 2801–2820.
[14] F. Mattioni, P.M. Weaver, M.I. Friswell, Multistable composite plates with piecewise variation of lay-up in the planform, International Journal of Solids and Structures 46 (1) (2009) 151–164.
[15] A. Pirrera, D. Avitabile, P.M. Weaver, Bistable plates for morphing structures: A refined analytical approach with high-order polynomials, International Journal of Solids and Structures 47 (25–26) (2010) 3412–3425.
[16] P. Portela, P. Camanho, P.M. Weaver, I. Bond, Analysis of morphing, multi stable structures actuated by piezoelectric patches, Computers and Structures 86 (3–5) (2008) 347–356.

[17] K.D. Potter, P.M. Weaver, A concept for the generation of out-of-plane distortion from tailored FRP laminates, Composites Part A: Applied Science and Manufacturing 35 (12) (2004) 1353–1361.
[18] M.S. Qatu, Vibration of Laminated Shells and Plates, Elsevier Publishing Company, 2004.
[19] M.R. Schultz, M.W. Hyer, Snap-through of unsymmetric cross-ply laminates using piezoceramic actuators, Journal of Intelligent Material Systems and Structures 14 (12) (2003) 795–814.
[20] A. Senba, T. Ikeda, T. Ueda, A two-way morphing actuation of bi-stable composites with piezoelectric fibers, in: 51st AIAA/ASME/ASCE/AHS/ASC Structures, Structural Dynamics and Materials Conference, 12–15 April 2010, Orlando, Florida, USA, 2010.
[21] SGL Group: The Carbon Company, High-performance prepregs: Preimpregnated products for fiber-reinforced composites, http://www.sglgroup.com, 2011.
[22] S.W. Tsai, H.T. Hahn, Introduction to Composite Materials, Technomic Publishing Company, Inc., 1980.
[23] D. Varelis, D.A. Saravanos, Coupled mechanics and finite element for non-linear laminated piezoelectric shallow shells undergoing large displacements and rotations, International Journal for Numerical Methods in Engineering 66 (8) (2006) 1211–1233.
[24] D. Varelis, D.A. Saravanos, Non-linear coupled multi-field mechanics and finite element for active multi-stable thermal piezoelectric shells, International Journal for Numerical Methods in Engineering 76 (1) (2008) 84–107.
[25] E. Ventsel, T. Krauthammer, Thin Plates and Shells: Theory: Analysis, and Applications, Marcel Dekker, Inc., 2001.
[26] G.A. Vogl, M.W. Hyer, Natural vibration of unsymmetric cross-ply laminates, Journal of Sound and Vibration 20 (330) (2011) 4764–4779.
[27] W.K. Wilkie, R.G. Bryant, J.W. High, R.L. Fox, R.F. Hellbaum, A. Jalink Jr., B.D. Little, P.H. Mirick, Low-cost piezocomposite actuator for structural control applications, in: 7th Annual International Symposium on Smart Structures and Materials, March 5–9, 2000, Newport Beach, CA, USA, 2000.